Walter+Eliza Hall
Institute of Medical Research

Research Publication Repository

http://publications.wehi.edu.au/search/SearchPublications

This is the author's peer reviewed manuscript version of a work accepted for publication.

Publication details:	Newton, K; Wickliffe, KE; Maltzman, A; Dugger, DL; Strasser, A; Pham, VC; Lill, JR; Roose-Girma, M; Warming, S; Solon, M; Ngu, H; Webster, JD; Dixit, VM. RIPK1 inhibits ZBP1-driven necroptosis during development. Nature 2016 540(7631):129-133.
Published version is available at:	https://doi.org/10.1038/nature20559

Changes introduced as a result of publishing processes such as copy-editing and formatting may not be reflected in this manuscript.

©2016 Macmillan Publishers Limited, part of Springer Nature.

RIPK1 inhibits ZBP1-driven necroptosis during development.

Kim Newton[1,*], Katherine E. Wickliffe[1], Allie Maltzman[1], Debra L. Dugger[1], Andreas Strasser[2], Victoria C. Pham[3], Jennie R. Lill[3], Merone Roose-Girma[4], Søren Warming[4], Margaret Solon[5], Joshua D. Webster[5], and Vishva M. Dixit[1,*]

Departments of Physiological Chemistry[1], Proteomics and Biological Resources[3], Molecular Biology[4], and Pathology[5], Genentech, 1 DNA Way, South San Francisco, CA 94080, USA.

[2] Molecular Genetics of Cancer Division, The Walter and Eliza Hall Institute of Medical Research, 1G Royal Parade, Parkville, VIC 3052, Australia

[*]Corresponding authors:

knewton@gene.com (ph: 1-650-225-8479)

dixit@gene.com (ph: 1-650-225-1312)

Main text: 1884 words

Abstract: 207 words

Methods: 797 words

Receptor interacting protein kinase 1 (RIPK1) promotes cell survival because mice lacking RIPK1 die perinatally, exhibiting aberrant caspase-8-dependent apoptosis and mixed lineage kinase-like (MLKL)-dependent necroptosis [1-3]. However, mice expressing catalytically inactive RIPK1 are viable [2,4,5], so an ill-defined pro-survival function for the RIPK1 scaffold has been proposed. Here we show that the RIP homotypic interaction motif (RHIM) in RIPK1 prevents the RHIM-containing adaptor protein ZBP1 (Z-DNA binding protein 1; also called DAI) from activating RIPK3 upstream of MLKL. *Ripk1*$^{RHIM/RHIM}$ mice expressing mutant RIPK1 with critical RHIM residues IQIG mutated to AAAA died around birth and exhibited RIPK3 autophosphorylation on Thr231 and Ser232, which is a hallmark of necroptosis [6]. Blocking necroptosis with catalytically inactive RIPK3 D161N, RHIM mutant RIPK3, RIPK3 deficiency, or MLKL deficiency prevented lethality in *Ripk1*$^{RHIM/RHIM}$ mice. Loss of ZBP1, which engages RIPK3 in response to certain viruses [7,8] but has no known role during development, also prevented perinatal lethality in *Ripk1*$^{RHIM/RHIM}$ mice. Consistent with the RHIM of RIPK1 functioning as a brake that prevents ZBP1 from engaging the RIPK3 RHIM, ZBP1 interacted with RIPK3 in *Ripk1*$^{RHIM/RHIM}$ *Mlkl*$^{-/-}$ macrophages, but not in wild-type, *Mlkl*$^{-/-}$ or *Ripk1*$^{RHIM/RHIM}$ *Ripk3*$^{RHIM/RHIM}$ macrophages. Collectively, these findings indicate that the RHIM of RIPK1 is critical for preventing ZBP1/RIPK3/MLKL-dependent necroptosis during development.

Studies of RIPK1 deficiency show that RIPK1 suppresses RIPK3/MLKL-dependent necroptosis in some cell types, and FADD/caspase-8-dependent apoptosis in others [1-3,9-12]. However, mutation of critical catalytic residues in RIPK1, or inhibition of RIPK1 enzymatic activity with the small molecule necrostatin-1, does not promote cell death [2,4,5,11,12]. Therefore, RIPK1 is hypothesized to form a pro-survival scaffold that is independent of its kinase activity. In addition to its kinase domain, RIPK1 has RHIM and death domain (DD) protein interaction motifs [13] (Fig. 1a). The DD mediates recruitment of RIPK1 to death receptors such as tumor necrosis factor receptor 1 (TNFR1) and to adaptor proteins such as Fas-associated via death domain (FADD), whereas the RHIM mediates interactions with RIPK3 [13]. To determine if the RHIM of RIPK1 is an essential part of the RIPK1 pro-survival scaffold, we generated *Ripk1*$^{RHIM/RHIM}$ mice with RHIM core residues IQIG [14] mutated to AAAA (Fig. 1a).

Ripk1$^{RHIM/RHIM}$ mice died around birth (Fig. 1b) with histologic lesions in the skin being the most striking and consistent phenotype (Fig. 1c). At embryonic day 18.5 (E18.5), the epidermis was hyperplastic and the underlying dermis was expanded by edema and infiltrated with leukocytes. Similar abnormalities in *Ripk1*$^{-/-}$ embryos require RIPK3 and MLKL-dependent necroptosis [1]. Of note, *Ripk1*$^{RHIM/RHIM}$ embryos lacked the caspase-8-dependent intestinal lesions seen in *Ripk1*$^{-/-}$ embryos [1] (Extended data fig. 1a). These data suggest that mutation of the RIPK1 RHIM primarily unleashes the RIPK3-MLKL necroptosis pathway (Extended data fig. 1b).

RIPK3 autophosphorylation on Thr231 and Ser232 is a hallmark of necroptosis [6]. A phospho-specific RIPK3 antibody recognizing these sites (Extended data fig. 1, c and d) stained many cells in the skin and thymus of *Ripk1*$^{RHIM/RHIM}$ embryos, but rare cells throughout multiple tissues including the bladder, liver, heart and intestine were also positive (Fig. 1c and Extended data fig. 1e). Importantly, staining was absent in wild-type (WT) embryos. RIPK3 autophosphorylation in the *Ripk1*$^{RHIM/RHIM}$ skin coincided with increased cell death based on TUNEL staining, which marks dying cells with DNA damage (Extended data fig. 1f), and cleaved caspase-3 staining, which marks apoptotic cells (Fig. 1c). Increased cell death was less evident in the *Ripk1*$^{RHIM/RHIM}$ thymus (Extended data fig. 1f), perhaps because MLKL was limiting. Thymocytes expressed considerably less MLKL than necroptosis-competent macrophages (Extended data fig. 1g).

Lethality and the skin lesions in *Ripk1*$^{RHIM/RHIM}$ mice were prevented by either RIPK3 or MLKL deficiency, suggesting these defects stemmed from aberrant necroptosis (Fig. 1c-f and Extended data fig. 2a-d). Although RIPK3 has been linked to apoptosis induction in some contexts [13], MLKL has not. Therefore, increased apoptosis in the *Ripk1*$^{RHIM/RHIM}$ dermis may have been a secondary consequence. *Ripk1*$^{RHIM/RHIM}$ *Ripk3*$^{+/-}$ mice were also viable and fertile, although 4 out of 7 mice developed severe dermatitis around the neck and ears after 6-9 months (Extended data fig. 2d). Sensitivity to *Ripk3* gene dosage was not unexpected because halving the *Ripk3* gene dosage also averts perinatal lethality in *Ripk1*$^{-/-}$ *Casp8*$^{-/-}$ mice [2]. *Ripk1*$^{RHIM/RHIM}$ mice expressing RIPK3 with RHIM residues VQIG mutated to AAAA (Extended data fig. 3a) or catalytically inactive RIPK3 D161N [4]

also survived beyond weaning, were fertile, and had no overt defects, albeit the eldest mice analyzed were only aged 3-6 months (Extended data fig. 3b-d). These data provide further support for necroptosis driving the lesions in *Ripk1*$^{RHIM/RHIM}$ mice because both the RHIM and kinase activity of RIPK3 are critical for necroptotic signaling (Extended data fig. 3e-h) [15-17].

RIPK1 deficiency compromises signaling by TNF in some cell types [9,18] so we compared WT, *Ripk1*$^{-/-}$, and *Ripk1*$^{RHIM/RHIM}$ primary mouse embryo fibroblasts (MEFs) after TNF treatment. Phosphorylation and degradation of IκBα, and phosphorylation of p38 and JNK were impaired in *Ripk1*$^{-/-}$ MEFs (Extended data fig. 4a) as reported [8], but occurred normally in *Ripk1*$^{RHIM/RHIM}$ MEFs (Extended data fig. 4b). *Ripk1*$^{RHIM/RHIM}$ MEFs treated with TNF also maintained normal levels of FLIP (FLICE-inhibitory protein), the adaptor protein TRAF2 (TNF receptor associated factor 2), and the ubiquitin ligase cIAP1 (cellular inhibitor of apoptosis protein 1), whereas these proteins were lost from *Ripk1*$^{-/-}$ MEFs (Extended data fig. 4c). Therefore, these RIPK1-dependent signaling events triggered by TNF in MEFs do not require the RIPK1 RHIM.

Next we examined necroptosis signaling in primary *Ripk1*$^{RHIM/RHIM}$ MEFs treated with TNF plus the pan-caspase inhibitor Z-VAD-FMK (hereafter abbreviated TZ). Similar to WT macrophages (Extended data fig. 3g and 4d), WT or *Ripk1*$^{RHIM/RHIM}$ MEFs exhibited RIPK1 phosphorylation on Ser166 after TZ treatment (Fig. 2a). We believe this modification represents RIPK1 autophosphorylation because it was absent when cells expressed catalytically inactive RIPK1 D138N. Interestingly, RIPK1 Ser166

112 phosphorylation was detected as early as 5 min after treatment with TNF or TZ (Fig. 2b),
113 indicating that it is not a necroptosis-specific modification. Analysis of the TNFR1-
114 associated signaling complex induced by TZ (Fig. 2c) indicated that WT, catalytically
115 inactive, or RHIM mutant RIPK1 were incorporated into the complex and modified in a
116 manner consistent with their being ubiquitylated [19]. However, only WT and RHIM
117 mutant RIPK1 were also phosphorylated on Ser166. Ubiquitylation of RIPK1 is thought
118 to contribute to TAK1 (Transforming growth factor β-activated kinase 1) and IKK
119 activation [20-24], so our data implying that RIPK1 autophosphorylation is dispensable for
120 RIPK1 ubiquitylation fits with TNF activating IKK- and TAK1-dependent signaling
121 pathways normally in *Ripk1*$^{D138N/D138N}$ cells [4] (Extended data fig. 5b).
122
123 We explored whether TNF-induced phosphorylation of RIPK1 Ser166 required RIPK1
124 ubiquitylation by pretreating WT MEFs with the IAP (inhibitor of apoptosis protein)
125 antagonist BV6 (Extended data fig. 5a) or by analyzing *Tradd*$^{-/-}$ macrophages (Extended
126 data fig. 5b). MEFs treated with BV6 lacked detectable cIAP1, consistent with BV6
127 inducing proteasomal degradation of the ubiquitin ligases cIAP1 and cIAP2 [25]. In
128 addition, RIPK1 associated with TNFR1 no longer migrated as a high molecular weight
129 smear, consistent with it being poorly ubiquitylated (Extended data fig. 5a). However,
130 RIPK1 phosphorylated on Ser166 was still detected, implying that RIPK1
131 autophosphorylation does not require RIPK1 ubiquitylation. Similar results were
132 obtained using *Tradd*$^{-/-}$ macrophages having reduced RIPK1 ubiquitylation in the TNFR1
133 signaling complex (Extended data fig. 5b). Collectively, our data suggest that RIPK1

associated with TNFR1 undergoes ubiquitylation and autophosphorylation with one modification not requiring the other.

TZ caused RIPK1 to interact with RIPK3 in WT MEFs, whereas TNF or Z-VAD-FMK alone did not (Extended data fig. 5c). Consistent with previous studies [15,16], this interaction required both the RHIM and kinase activity of RIPK1 (Fig. 2a). RIPK1 interacting with RIPK3 promotes RIPK3 oligomerization and autophosphorylation [26]. Therefore, as expected, TZ induced RIPK3 autophosphorylation in WT MEFs, but not in *Ripk1*$^{D138N/D138N}$ MEFs (Fig. 2a). RIPK3 was not autophosphorylated in WT MEFs treated with TNF or Z-VAD-FMK individually (Fig. 2d). Strikingly, both *Ripk1*$^{RHIM/RHIM}$ and *Ripk1*$^{-/-}$ MEFs exhibited RIPK3 autophosphorylation in medium alone (Fig. 2a and Extended data fig. 5d). These data indicate that the RHIM of RIPK1 suppresses RIPK3 activation in primary MEFs as well as in the skin and thymus of the developing mouse. RIPK3 autophosphorylation in the *Ripk1*$^{RHIM/RHIM}$ or *Ripk1*$^{-/-}$ MEFs did not induce significant cell death (Extended data fig. 5e), although it should be noted that WT MEFs were also considerably less sensitive to TZ than macrophages (Extended data fig. 3e) or immortalized MEFs [4]. Primary MEFs, like thymocytes, expressed less MLKL than macrophages (Extended fig. 1g) and this may contribute to their relative insensitivity to RIPK3 activation.

How might the RIPK1 RHIM suppress RIPK3 activation when interactions between RIPK1 and RIPK3 were only detected after TZ treatment (Fig. 2 and Extended data fig. 5c)? Furthermore, does an upstream stimulus drive RIPK3 activation in *Ripk1*$^{-/-}$ or

157 *Ripk1*$^{RHIM/RHIM}$ cells, or does RIPK3 above a threshold level activate spontaneously? Two
158 other RHIM-containing proteins besides RIPK1 and RIPK3 are ZBP1 and TRIF.
159 Therefore, we tested if loss of both ZBP1 and TRIF substituted for RIPK3 deficiency and
160 rescued lethality in *Ripk1*$^{-/-}$ *Casp8*$^{-/-}$ mice [1-3]. After intercrossing *Ripk1*$^{+/-}$ *Casp8*$^{+/-}$ *Zbp1*$^{-/-}$
161 *Trif*$^{-/-}$ mice, we obtained viable *Ripk1*$^{-/-}$ *Casp8*$^{-/-}$ *Zbp1*$^{-/-}$ *Trif*$^{-/-}$ mice with a median survival
162 of 17 weeks, whereas *Ripk1*$^{-/-}$ *Casp8*$^{+/+}$ *Zbp1*$^{-/-}$ *Trif*$^{-/-}$ or *Ripk1*$^{-/-}$ *Casp8*$^{+/-}$ *Zbp1*$^{-/-}$ *Trif*$^{-/-}$
163 littermates died within 3 weeks (Fig. 3, a and b). With the exception of two mice with
164 severe malocclusion, all weaned *Ripk1*$^{-/-}$ *Casp8*$^{-/-}$ *Zbp1*$^{-/-}$ *Trif*$^{-/-}$ mice were euthanized due
165 to lymphadenopathy from the accumulation of CD3^{+} B220^{+} T cells (Fig. 3, c and d), a
166 known consequence of caspase-8 deficiency [27]. Lymphadenopathy was accompanied by
167 significantly elevated serum IL-17A and CCL4/MIP-1β (Extended data fig. 6a). The
168 only other consistent phenotype revealed by histological analysis of all the major organ
169 systems at 3-6 months of age was testicular atrophy in the *Ripk1*$^{-/-}$ *Casp8*$^{-/-}$ *Zbp1*$^{-/-}$ *Trif*$^{-/-}$
170 males (Extended data fig. 6b).
171
172 Survival of *Ripk1*$^{-/-}$ *Casp8*$^{-/-}$ *Zbp1*$^{-/-}$ *Trif*$^{-/-}$ mice beyond weaning suggests that ZBP1 and/or
173 TRIF promote RIPK3 activation when RIPK1 is absent. Consistent with this notion,
174 E18.5 *Ripk1*$^{-/-}$ *Zbp1*$^{-/-}$ *Trif*$^{-/-}$ skin had few cells containing autophosphorylated RIPK3
175 when compared to *Ripk1*$^{-/-}$ skin (Fig. 3e). Epidermal hyperplasia and dermatitis were still
176 evident in *Ripk1*$^{-/-}$ *Zbp1*$^{-/-}$ *Trif*$^{-/-}$ skin, but presumably this was due to caspase-8-dependent
177 apoptosis because neither occurred in the skin of *Ripk1*$^{-/-}$ *Casp8*$^{-/-}$ *Zbp1*$^{-/-}$ *Trif*$^{-/-}$ mice aged
178 3-6 months (Extended data fig. 6c). One *Ripk1*$^{-/-}$ *Casp8*$^{-/-}$ *Zbp1*$^{-/-}$ mouse was obtained
179 from limited intercrossing of *Ripk1*$^{+/-}$ *Casp8*$^{+/-}$ *Zbp1*$^{+/-}$ *Trif*$^{+/-}$ mice and it lacked overt

defects at 7 weeks of age (Extended data fig. 6d). Thus, ZBP1 potentially contributes more than TRIF to *Ripk1*$^{-/-}$ perinatal lethality. Consistent with this idea, ZBP1 deficiency alone rescued perinatal lethality in the *Ripk1*$^{RHIM/RHIM}$ mice, whereas TRIF deficiency did not (Fig. 4a-c and Extended data fig. 7a). *Ripk1*$^{RHIM/RHIM}$ *Zbp1*$^{-/-}$ mice aged 7 weeks lacked histologic skin lesions but they still exhibited some RIPK3 autophosphorylation in the dermis (Fig. 4d and Extended data fig. 7b). Therefore, it is possible that TRIF-dependent RIPK3 activation might elicit lesions in older *Ripk1*$^{RHIM/RHIM}$ *Zbp1*$^{-/-}$ mice.

We sought biochemical evidence for ZBP1 or TRIF engaging RIPK3 in *Ripk1*$^{RHIM/RHIM}$ macrophages, but found that *Ripk1*$^{RHIM/RHIM}$ fetal liver cells cultured with M-CSF yielded approximately 5-fold fewer Mac-1^{+} F4/80^{+} macrophages than their WT counterparts (Extended data fig. 7c). Furthermore, *Ripk1*$^{-/-}$ or *Ripk1*$^{RHIM/RHIM}$ macrophages contained abnormally low amounts of ZBP1, RIPK3 and MLKL (Extended data fig. 7d), suggesting selection for cells unable to die. To circumvent these issues, we analyzed *Ripk1*$^{RHIM/RHIM}$ *Mlkl*$^{-/-}$ bone marrow-derived macrophages. No interaction between RIPK3 and TRIF was detected, but RIPK3 did coimmunoprecipitate with ZBP1 (Fig. 4e). No RIPK3/ZBP1 interaction occurred in WT, *Mlkl*$^{-/-}$, or *Ripk1*$^{RHIM/RHIM}$ *Ripk3*$^{RHIM/RHIM}$ macrophages, indicating that ZBP1 engages the RIPK3 RHIM only when the RIPK1 RHIM is mutated. We explored whether RIPK1 might sequester ZBP1 in WT cells and thereby prevent it from interacting with RIPK3, but failed to detect a RIPK1/ZBP1 interaction. Therefore, how the RIPK1 RHIM suppresses the ZBP1/RIPK3 interaction remains enigmatic.

ZBP1 has two N-terminal Z-DNA binding domains in addition to its C-terminal RHIMs [28], and promotes necroptosis in response to murine cytomegalovirus [7] or influenza [8] infection. However, it is unclear if ZBP1 acts as a DNA sensor during infection. ZBP1 is also a type I interferon-inducible gene [29]. ZBP1 was more abundant in E18.5 *Ripk1*$^{RHIM/RHIM}$ skin (Extended data fig. 7e), but this did not (?) coincide with a marked increase in *Ifnb* expression (Extended data fig. 7f). ZBP1 was not increased in *Ripk1*$^{RHIM/RHIM}$ *Ripk3*$^{-/-}$ or *Ripk1*$^{RHIM/RHIM}$ *Mlkl*$^{-/-}$ skin, so it is possible that *Ripk1*$^{RHIM/RHIM}$ skin contained more ZBP1 because of infiltrating leukocytes. Immune cells undergoing necroptosis may also have enhanced RIPK3 autophosphorylation in *Ripk1*$^{RHIM/RHIM}$ skin compared to *Ripk1*$^{RHIM/RHIM}$ *Mlkl*$^{-/-}$ skin (Fig. 1c and 4f).

In sum, our analyses have revealed an unexpected role for ZBP1 in triggering necroptosis in the perinatal period. Future studies will need to address if ZBP1 senses viral infections and/or DNA in this context, or if mutation of the RIPK1 RHIM is necessary and sufficient for ZBP1/RIPK3 interactions that induce necroptosis.

References

1 Rickard, J. A. *et al*. RIPK1 regulates RIPK3-MLKL-driven systemic inflammation and emergency hematopoiesis. *Cell* **157**, 1175-1188 (2014)

2 Kaiser, W. J. *et al*. RIP1 suppresses innate immune necrotic as well as apoptotic cell death during mammalian parturition. *PNAS* **111**, 7753-7758 (2014)

3 Dillon, C. P. *et al*. RIPK1 blocks early postnatal lethality mediated by caspase-8 and RIPK3. *Cell* **157**, 1189-1202 (2014)

4 Newton, K. *et al*. Activity of protein kinase RIPK3 determines whether cells die by necroptosis or apoptosis. *Science* **343**, 1357-1360 (2014)

5 Polykratis, A. *et al*. Cutting edge: RIPK1 Kinase inactive mice are viable and protected from TNF-induced necroptosis in vivo. *J. Immunol*. **193**, 1539-1543 (2014)

6 Chen, W. *et al*. Diverse sequence determinants control human and mouse receptor interacting protein 3 (RIP3) and mixed lineage kinase domain-like (MLKL) interaction in necroptotic signaling. *J. Biol. Chem*. **288**, 16247-16261 (2013)

7 Upton, J. W., Kaiser, W. J. & Mocarski, E. S. DAI/ZBP1/DLM-1 complexes with RIP3 to mediate virus-induced programmed necrosis that is targeted by murine cytomegalovirus vIRA. *Cell Host Microbe* **11**, 290-297 (2012)

8 Kuriakose, T. *et al*. ZBP1/DAI is an innate sensor of influenza virus triggering the NLRP3 inflammasome and programmed cell death pathways. *Sci. Immunol*. **1**, aag2045 (2016)

9 Dannappel, M. *et al*. RIPK1 maintains epithelial homeostasis by inhibiting apoptosis and necroptosis. *Nature* **513**, 90-94 (2014)

10 Takahashi, N. *et al*. RIPK1 ensures intestinal homeostasis by protecting the epithelium against apoptosis. *Nature* **513**, 95-99 (2014)

11 Kearney, C. J., Cullen, S. P., Clancy, D. & Martin, S. J. RIPK1 can function as an inhibitor rather than an initiator of RIPK3-dependent necroptosis. *FEBS J*. **281**, 4921-4934 (2014)

12 Orozco, S. *et al*. RIPK1 both positively and negatively regulates RIPK3 oligomerization and necroptosis. *Cell Death Differ*. **21**, 1511-1521 (2014)

13 Newton, K. & Manning, G. Necroptosis and Inflammation. *Ann. Rev. Biochem*., doi:10.1146/annurev-biochem-060815-014830 (2016)

14 Sun, X., Yin, J., Starovasnik, M. A., Fairbrother, W. J. & Dixit, V. M. Identification of a novel homotypic interaction motif required for the phosphorylation of receptor-interacting protein (RIP) by RIP3. *J. Biol. Chem*. **277**, 9505-9511 (2002)

15 Cho, Y. S. *et al*. Phosphorylation-driven assembly of the RIP1-RIP3 complex regulates programmed necrosis and virus-induced inflammation. *Cell* **137**, 1112-1123 (2009)

16 He, S. *et al*. Receptor interacting protein kinase-3 determines cellular necrotic response to TNF-alpha. *Cell* **137**, 1100-1111 (2009)

17 Zhang, D. W. *et al*. RIP3, an energy metabolism regulator that switches TNF-induced cell death from apoptosis to necrosis. *Science* **325**, 332-336 (2009)

18 Kelliher, M. A. *et al*. The death domain kinase RIP mediates the TNF-induced NF-kappaB signal. *Immunity* **8**, 297-303 (1998)

19 Newton, K. *et al*. Ubiquitin chain editing revealed by polyubiquitin linkage-specific antibodies. *Cell* **134**, 668-678 (2008)

20 Ea, C. K., Deng, L., Xia, Z. P., Pineda, G. & Chen, Z. J. Activation of IKK by TNFalpha requires site-specific ubiquitination of RIP1 and polyubiquitin binding by NEMO. *Mol. Cell* **22**, 245-257 (2006)

21 Bertrand, M. J. *et al*. cIAP1 and cIAP2 facilitate cancer cell survival by functioning as E3 ligases that promote RIP1 ubiquitination. *Mol. Cell* **30**, 689-700 (2008)

22 Varfolomeev, E. *et al*. c-IAP1 and c-IAP2 are critical mediators of tumor necrosis factor alpha (TNFalpha)-induced NF-kappaB activation. *J. Biol. Chem*. **283**, 24295-24299 (2008)

23 Ermolaeva, M. A. *et al*. Function of TRADD in tumor necrosis factor receptor 1 signaling and in TRIF-dependent inflammatory responses. *Nat. Immunol*. **9**, 1037-1046 (2008)

24 Pobezinskaya, Y. L. *et al*. The function of TRADD in signaling through tumor necrosis factor receptor 1 and TRIF-dependent Toll-like receptors. *Nat. Immunol*. **9**, 1047-1054 (2008)

25 Varfolomeev, E. *et al*. IAP antagonists induce autoubiquitination of c-IAPs, NF-kappaB activation, and TNFalpha-dependent apoptosis. *Cell* **131**, 669-681 (2007)

26 Wu, X. N. *et al*. Distinct roles of RIP1-RIP3 hetero- and RIP3-RIP3 homo-interaction in mediating necroptosis. *Cell Death and Differ*. **21**, 1709-1720 (2014)

27 Salmena, L. & Hakem, R. Caspase-8 deficiency in T cells leads to a lethal lymphoinfiltrative immune disorder. *J. Exp. Med*. **202**, 727-732 (2005)

28 Kaiser, W. J., Upton, J. W. & Mocarski, E. S. Receptor-interacting protein homotypic interaction motif-dependent control of NF-kappa B activation via the DNA-dependent activator of IFN regulatory factors. *J. Immunol.* **181**, 6427-6434 (2008)

29 Takaoka, A. *et al.* DAI (DLM-1/ZBP1) is a cytosolic DNA sensor and an activator of innate immune response. *Nature* **448**, 501-505 (2007)

Acknowledgments

We thank Jose Diaz, Michael Long, Claire Allen, Martin Garcia, Alexandra Verducci and Jerome Anunciacion for animal husbandry, Robert Newman, Margaret Solon and members of the Genentech genetic analysis and histology laboratories for technical assistance, and Joyce Lai and Scott Stawicki for antibody project management.

Author contributions

MRG and SW generated the *Ripk1*$^{RHIM/+}$ and *Ripk3*$^{RHIM/+}$ mice, KN, AM, DLD, KEW, MS and AS designed and performed experiments, VCP and JRL characterized the RIPK1 and RIPK3 autophosphorylation sites, JDW analyzed histological data, and VMD helped with experimental design.

Author information

Reprints and permissions information is available at www.nature.com/reprints. All authors were employees or visiting scientists of Genentech. Correspondence and requests for materials should be addressed to dixit@gene.com or knewton@gene.com.

Figure Legends

Figure 1. Mutation of the RIPK1 RHIM causes RIPK3/MLKL-dependent lethality.

(a) Organization of the *Ripk1*^{RHIM} mutant allele. Black boxes indicate exons. DD, death domain. RHIM, RIP homotypic interaction motif.

(b) Numbers of offspring from *Ripk1*$^{RHIM/+}$ parents. Strains 1 and 2 were derived from independent ES cell clones.

(c) E18.5 embryo sections. Cells containing autophosphorylated RIPK3 (p-RIPK3) or cleaved caspase-3 by immunohistochemistry (IHC) stained brown. H & E, hematoxylin and eosin. Scale bars, 100 μm. Results are representative of 3-5 embryos of each genotype.

(d and e) Numbers of offspring from compound heterozygote parents that survived beyond weaning at ~ 21 days.

(f) Kaplan-Meier plot of mouse survival. Mice were either found dead (&) or euthanized because of an enlarged abdomen (#) or skin lesions (*).

Figure 2. The RIPK1 RHIM is dispensable for RIPK1 autophosphorylation but mediates interactions with RIPK3 in response to TZ.

(a-d) Western blots of MEFs or immunoprecipitations (IP) performed with the indicated antibodies. T, TNF. Z, Z-VAD-FMK. p-RIPK1, phosphorylated RIPK1 Ser166. p-RIPK3, phosphorylated RIPK3 Thr231 and Ser232. Asterisks indicate non-specific bands. Results are representative of 2 (c), 4 (a and b) or 5 (d) independent experiments.

Figure 3. Combined ZBP1 and TRIF deficiency rescues perinatal lethality in *Ripk1*$^{-/-}$ *Casp8*$^{-/-}$ mice.

(a) Numbers of offspring of *Ripk1*$^{+/-}$ *Casp8*$^{+/-}$ *Zbp1*$^{-/-}$ *Trif*$^{/-}$ parents.

(b) Kaplan-Meier plot of mouse survival. Note that animals clipped at P3-P6 and not found at weaning were recorded as dead at 21 d, but may have died earlier.

(c) Spleen and lymph nodes (mesenteric, brachial, and inguinal) of male littermates aged 18 weeks.

(d) Flow cytometric analysis of lymph node cells from female mice aged 15-17 weeks.

(e) E18.5 skin sections. Cells containing autophosphorylated RIPK3 (p-RIPK3) by immunohistochemistry (IHC) stained brown. Scale bar, 100 μm.

Results in (c-e) are representative of 3-4 mice of each genotype.

Figure 4. ZBP1 interacts with RIPK3 to trigger necroptosis in *Ripk1*$^{RHIM/RHIM}$ mice.

(a and b) Numbers of offspring from compound heterozygote parents that survived beyond weaning at ~ 21 days.

(c) Kaplan-Meier plot of mouse survival.

(d) Skin sections from female littermates aged 7 weeks. Cells containing autophosphorylated RIPK3 (p-RIPK3) by immunohistochemistry (IHC) stained brown. Scale bar, 100 μm. Results are representative of 2 *Ripk1*$^{RHIM/RHIM}$ *Zbp1*$^{-/-}$ mice.

(e) Western blots of macrophages or immunoprecipitates (IP). Results are representative of 4 independent experiments.

Methods

Mice

Ripk3$^{-/-}$ [4], *Ripk3*$^{D161N/D161N}$ [4], *Ripk1*$^{D138N/D138N}$ [4], *Ripk1*$^{-/-}$ [4], *Casp8*$^{-/-}$ [4], *Tradd*$^{-/-}$ [22], *Mlkl*$^{-/-}$ [30], *Zbp1*$^{-/-}$ [31], and *Trif*$^{/-}$ [32] mice were described previously. A second *Zbp1*$^{-/-}$ strain generated by Taconic (Germany) using C57BL/6NTac ES cells was also crossed to *Ripk1*$^{RHIM/RHIM}$ mice and rescued perinatal lethality similar to the published *Zbp1*$^{-/-}$ strain [31] so results were pooled. The Taconic strain lacked the *Zbp1* 5' UTR and exon 1 corresponding to NCBI37/mm9 chr2:173,043,537-173,045,687. *Ripk1*$^{RHIM/+}$ and *Ripk3*$^{RHIM/+}$ mice were generated at Genentech using C57BL/6N C2 ES cells. A *FRT*-flanked neomycin selection cassette inserted upstream of *Ripk1* exon 10 at position chr13:34,029,090 (GRCm38/mm10 assembly) or upstream of *Ripk3* exon 10 at position chr14:55,785,501 (reverse strand) was deleted from the targeted ES cells prior to microinjection by adenoviral delivery of Flpe. *Ripk1* sequence ATT CAG ATT GGA encoding RHIM residues IQIG was replaced with the sequence GCT GCG GCT GCA. *Ripk3* sequence GTG CAG ATT GGG encoding RHIM residues VQIG was replaced with the sequence GCA GCC GCG GCT.

Ripk1^{RHIM} genotyping primers 5’ CCA CAT TCT TGC CAA CAC TG and 5’ GCA AGT ATT GTT TGG TGG TTG amplified 299 base pair (bp) wild-type and 333 bp knock-in DNA fragments. *Ripk3*^{RHIM} genotyping primers 5’ AGC AGG CAC TAC TCT TTG AGC T and 5’ CTG TGC TTG GTC ATA CTT GGC amplified 325 bp wild-type and 359 bp knock-in DNA fragments. *Zbp1* genotyping primers 5’ AGA CCA TTA GAA AGC ACA GAT C, 5’ TGG CCT CTC CTT CAT TCC and 5’ CTC CTA GGT CAG

TGA CTC TC amplified 145 bp wild-type and 294 bp knock-out (Taconic strain) DNA fragments.

For timed pregnancies, mice were designated E0.5 on the morning a vaginal plug was detected. When determining offspring numbers, pups were clipped between 3-6 days of age. The Genentech institutional animal care and use committee approved all protocols.

Immunohistochemistry

Formalin-fixed, paraffin-embedded tissue sections were stained with 5 μg/ml rabbit anti-mouse phospho-RIPK3 antibody (GEN135-35-9, Genentech) recognizing phosphorylated residues Thr231, Ser232. Immunohistochemistry was performed on the Ventana Discovery XT platform with CC1 standard antigen retrieval. The reaction was detected with the HQ amplification system using DAB as the chromogen and hematoxylin counterstain. Josh to insert CC3 IHC and TUNEL staining methods.

Cell culture

Primary MEFs isolated from E13.5 or E14.5 embryos were grown in the high glucose version of Dulbecco's Modified Eagle Medium (DMEM) supplemented with 10% heat inactivated-fetal bovine serum, 2 mM glutamine, 10 mM HEPES (pH 7.2), 1X non-essential amino acids solution, 100 U/ml penicillin, and 100 μg/ml streptomycin on tissue culture dishes pre-coated with 0.1% gelatin in PBS. Primary macrophages were differentiated from bone marrow cells in non-treated plates using the same medium supplemented with 25 ng/ml M-CSF (R&D Systems) for 5-6 d. Bone marrow-derived

399 macrophages (BMDMs) were then harvested and replated for experiments. BMDMs and
400 MEFs were stimulated with 100 ng/ml murine TNF (Genentech), 20 μM Z-VAD-FMK
401 (Promega), 100 ng/ml ultra-pure LPS-EB (Invivogen), 50 μg/ml LMW poly I-C
402 (Invivogen), 2 μM BV6 (Genentech), 1 μg/ml ^{Flag}TNF (Enzo Life Sciences) or 20 μg/ml
403 cycloheximide (Sigma). BMDM viability was assessed after YOYO-1 (Molecular
404 Probes) staining and live cell imaging in an Incucyte system (Essen Bioscience).
405 Alternatively, BMDMs were harvested from non-treated plates with a cell scraper into the
406 culture medium along with any floating dead cells, stained with 2.5 μg/ml propidium
407 iodide (PI; BD Biosciences), and analyzed in a FACSCanto II (BD Biosciences).
408
409 E14.5 fetal liver cells were plated overnight in high glucose DMEM supplemented with
410 10% heat inactivated-fetal bovine serum, 2 mM glutamine, 100 μM asparagine, 55 μM 2-
411 mercaptoethanol, 50 U/ml penicillin, and 50 μg/ml streptomycin. 2.5 x 10^6 viable,
412 nucleated, non-adherent cells were then plated on a 15 cm non-treated dish in 50 ng/ml
413 M-CSF (R&D Systems) for 7 days. Adherent cells were harvested with a cell scraper,
414 counted, and then analyzed by flow cytometry after staining with antibodies recognizing
415 FITC-conjugated MCA497, CI:A3-1 anti-F4/80 (Bio-Rad), PE-conjugated M1/70 anti-
416 Mac-1 (BD Biosciences), and APC-conjugated RB6-8C5 anti-Gr-1 (BD Biosciences).
417 Dead cells that stained with PI were excluded from analyses.
418
419 Lymph node cells were stained with FITC-conjugated 145-2C11 anti-CD3 (BD
420 Biosciences) and APC-conjugated RA3-6B2 anti-B220 (BD Biosciences) antibodies for
421 flow cytometric analysis. Dead cells that stained with PI were excluded from analyses.

To test the specificity of the GEN135-35-9 anti-phospho-RIPK3 antibody, 293T cells (ATCC) were transfected with N-terminal 3xFlag-tagged mouse RIPK3 variants in vector pCMV-3Tag-6 (Agilent) using lipofectamine 2000 (ThermoFisher).

Immunoprecipitation and western blotting

Cells were lysed in 20 mM Tris.HCl pH 7.5, 135 mM NaCl, 1.5 mM $MgCl_2$, 1 mM EGTA, 1% Triton X-100, 10% glycerol, phosSTOP phosphatase inhibitor (Roche), and complete protease inhibitor cocktail (Roche) (Figure 2 and Extended data fig. 1c, 3, 4a-c, 5 and 7g). Insoluble material was removed by centrifugation at 14,000 rpm prior to immunoprecipitation or addition of LDS sample buffer. Alternatively, cells were lysed in 10 mM Tris.HCl pH 7.5, 150 mM NaCl, 2.5 mM $MgCl_2$, 0.5 mM $CaCl_2$, 1% NP40, phosphatase/protease inhibitors (Roche) and DNase (~80 U/ml, Qiagen) (Extended data fig. 1d, 4d and 7f). The whole cell lysate was denatured directly in LDS sample buffer.

Immunoprecipitating antibodies recognized RIPK1 (cat#610459, BD Biosciences), RIPK3 (cat#NBP1-77299, Novus Biologicals), ZBP1 (clone Zippy-1, Adipogen), FLAG (clone M2, Sigma), or were irrelevant control IgGs (Mouse IgG2a, BD Biosciences, 553454; or Rabbit IgG, Millipore, 12-370). Antibody complexes were recovered with magnetic protein A/G beads (Pierce) or magnetic FLAG beads (Sigma).

Western blot antibodies recognized RIPK3 (1G6.1.4, Genentech), phosphorylated RIPK3 Thr231, Ser232 (GEN135-35-9 raised against peptide ELVDK(pT)(pS)LIRET,

Genentech), RIPK1 (BD Biosciences), phosphorylated RIPK1 Ser166 (GEN150-33-4 raised against peptide GVASFKTW(pS)KLTKEK, Genentech), FLAG (clone M2, Sigma), β-actin (MP Biomedicals, mouse clone C4), FADD (1.28E12, Genentech), caspase-8 (1G12, Enzo Life Sciences), FLIP (2.21H2, Genentech), MLKL (1G12, Genentech), TRAF2 (cat#7187, Santa Cruz Biotechnology), cIAP1 (cat#ALX-803-335-C100, Enzo Life Sciences), and TRADD (GN-21-3, Genentech). The following antibodies were from Cell Signaling Technologies: p-ERK (cat#9101), ERK (cat#9102), p-JNK (cat#4668), JNK (cat#9258), p-IκBα (cat#2859), IκBα (cat#9242), p-p65/RelA (cat#3033), p65/RelA (cat#8242), p-p38 (cat#9211), and p38 (cat#8690). RIPK3 antibody 1G6 was biotinylated using a Biotin-xx Microscale Protein Labeling Kit (Molecular Probes) in order to detect RIPK3 in ZBP1 immunoprecipitates.

Chemokines and cytokines

E18.5 mouse skin was homogenized in ice-cold 50 mM Tris HCl pH 7.4, 150 mM NaCl, 2 mM EDTA, 0.5% sodium deoxycholate, 0.1% SDS, 1% NP-40, and 1 mM DTT supplemented with complete protease inhibitor cocktail (Roche). Insoluble material was pelleted at 20,000xg and the protein concentration in the soluble fraction measured by Bio-rad Protein Assay. Skin lysates adjusted to 1 mg protein/ml or sera were analysed by Bio-Plex Pro Mouse Cytokine 23-plex (Bio-Rad).

References

30 Murphy, J. M. *et al*. The pseudokinase MLKL mediates necroptosis via a molecular switch mechanism. *Immunity* **39**, 443-453 (2013)

31 Ishii, K. J. *et al*. TANK-binding kinase-1 delineates innate and adaptive immune responses to DNA vaccines. *Nature* **451**, 725-729 (2008)

32 Yamamoto, M. *et al*. Role of adaptor TRIF in the MyD88-independent toll-like receptor signaling pathway. *Science* **301**, 640-643 (2003)

475 **Extended Data Figure Legends**

476

477 **Extended data figure 1. Characterization of *Ripk1* mutant mice with a monoclonal**
478 **antibody recognizing autophosphorylated RIPK3.**

479 (a) E17.5 colon sections stained with hematoxylin and eosin. Scale bar, 100 μm. Results
480 are representative of 3 mice of each genotype.

481 (b) Model for RIPK3 activation following mutation of the RIPK1 RHIM.

482 (c) Western blots of HEK293T cells transfected with Flag-tagged mouse RIPK3 variants,
483 overexpression being sufficient to activate RIPK3 autophosphorylation on Thr231 and
484 Ser232 based on mass spectrometry (data not shown). p-RIPK3, RIPK3 phosphorylated
485 on Thr231, Ser232.

486 (d) Western blots of macrophages at 4 h after treatment. T, TNF. Z, Z-VAD-FMK.
487 Results are representative of 5 independent experiments.

488 (e and f) E18.5 embryo sections. In (e), cells containing autophosphorylated RIPK3 are
489 stained brown (rare positive cells are indicated by arrows). In (f), dying cells that are
490 TUNEL-positive are black. Scale bar, 50 μm (except the skin and thymus, which have a
491 100 μm scale bar). Results are representative of 3-5 mice of each genotype. Graph in (f)
492 indicates quantification of p-RIPK3, cleaved caspase-3, and TUNEL staining in the E18.5
493 skin and thymus.

494 (g) Western blots of WT bone marrow-derived macrophages (BMDMs), MEFs, and adult
495 mouse thymus. Results are representative of 2 independent experiments.

496

Extended data figure 2. Characterization of *Ripk1*$^{RHIM/RHIM}$ mice lacking RIPK3 or MLKL.

(a) E18.5 skin cytokines and chemokines. Bars indicate the mean ± s.e.m. n=5 embryos of each genotype. Asterisks indicate significant differences in *Ripk1*$^{RHIM/RHIM}$ skin compared to WT by student t-test. * $p<0.05$, ** $p<0.01$, ***$p<0.001$.

(b) Body weights of mice aged 7-8 months. Each symbol represents one mouse. Lines indicate the mean.

(c) Serum cytokines and chemokines of mice aged 8-12 months. Bars indicate the mean ± s.e.m of 3 females and 3 males of each genotype.

(d) Hematoxylin and eosin stained skin sections of female mice aged 9 months. Scale bar, 100 μm. Results are representative of 3-4 WT, *Ripk1*$^{RHIM/RHIM}$ *Ripk3*$^{-/-}$, and *Ripk1*$^{RHIM/RHIM}$ *Mlkl*$^{-/-}$ male or female mice.

Extended data figure 3. *Ripk1*$^{RHIM/RHIM}$ mice expressing catalytically inactive or RHIM mutant RIPK3 are viable.

(a) Organization of the *Ripk3*^{RHIM} mutant allele. Black boxes indicate exons. RHIM, RIP homotypic interaction motif.

(b and c) Numbers of offspring from compound heterozygote parents that survived beyond weaning at ~ 21 days.

(d) Kaplan-Meier plot of mouse survival.

(e) Graph indicates the percentage of macrophages that are viable and not stained by propidium iodide (PI^{neg}) at 16 h after treatment. T, TNF. L, LPS. P, poly I-C. Z, Z-

VAD-FMK. Bars are the mean ± s.e.m. Cells from 3 mice of each genotype were analyzed.

(f) Representative images of macrophages stained with YOYO-1 at 16 h after the same treatments as in (e). Note that this assay does not reveal death in response to TNF, LPS or poly I-C individually. Therefore, the death quantified in (e) due to TNF, LPS or poly I-C individually is probably linked to mechanical scraping of the cells prior to flow cytometry.

(g and h) Western blots of macrophages. Results are representative of 2 independent experiments.

Extended data figure 4. Comparison of *Ripk1*$^{-/-}$ and *Ripk1*$^{RHIM/RHIM}$ MEFs.

(a-d) Western blots of MEFs (a-c) or macrophages (d). p- indicates an active, phosphorylated variant of the protein. Results are representative of 2 (b), 3 (a) or 5 (d) independent experiments.

Extended data figure 5. Biochemical analyses of RIPK1 following TNF stimulation.

(a-d) Western blots of MEFs (a, c and d) or macrophages (b). MEFs in (a) that received BV6 were pretreated for 2 h prior to stimulation with ^{Flag}TNF. In (d), MEFs derived from 3 different embryos of each genotype were analyzed.

(e) Graph indicates the percentage of primary MEFs that are viable and not stained by propidium iodide (PI^{neg}) at 25 h after treatment. T, TNF. Z, Z-VAD-FMK. C, cycloheximide. Each symbol represents cells from a different embryo. Lines indicate the mean.

Extended data figure 6. Characterization of *Ripk1*$^{-/-}$ *Casp8*$^{-/-}$ *Trif*$^{-/-}$ *Zbp1*$^{-/-}$ mice.

(a) Serum cytokines and chemokines of mice aged 4-5 weeks (upper graph) or 3-6 months (lower graph). Bars indicate the mean ± s.e.m of 3-4 mice of each genotype. Asterisks indicate significantly different amounts by students t-test ($p<0.05$).

(b) Hematoxylin and eosin stained testes sections from mice aged 12 weeks. Scale bar, 100 μm. Results are representative of two *Ripk1*$^{-/-}$ *Casp8*$^{-/-}$ *Trif*$^{-/-}$ *Zbp1*$^{-/-}$ males.

(c) Hematoxylin and eosin stained skin sections from female littermates aged 19 weeks. Scale bar, 100 μm. Results are representative of three *Ripk1*$^{-/-}$ *Casp8*$^{-/-}$ *Trif*$^{-/-}$ *Zbp1*$^{-/-}$ mice.

(d) Skin sections from male mice aged 7 weeks.

Extended data figure 7. The effect of DAI and/or TRIF deficiency on *Ripk1*$^{RHIM/RHIM}$ mice.

(a) E18.5 skin sections. Scale bar, 100 μm. Results are representative of 3 embryos of each genotype.

(b) Western blots of skin from mice aged 6-8 weeks.

(c) Graph indicates the number of F4/80^{+} Mac-1^{+} macrophages obtained after 2.5 x 10^{6} E14.5 viable, nucleated fetal liver cells were cultured in M-CSF for 7 days. Each symbol represents cells from one embryo. Lines indicate the mean.

(d) Western blot analysis of the macrophages in (d). Cells from two embryos of each genotype were analyzed.

(f) Western blot analysis of E18.5 skin. Three embryos of each genotype were analyzed.

(g) Graph indicates *Ifnb* gene expression in E18.5 skin. Bars are the mean ± s.e.m. n=?

a

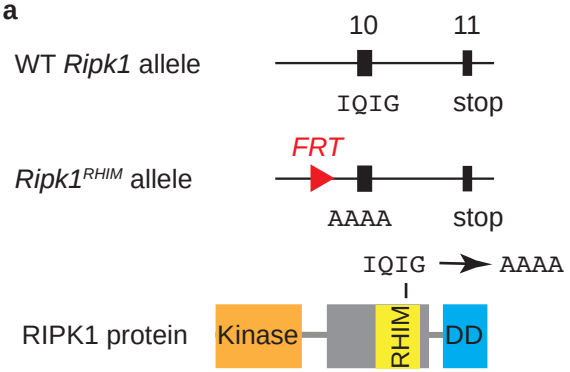

b

Strain	*Ripk1*$^{+/+}$	*Ripk1*$^{+/RHIM}$	*Ripk1*$^{RHIM/RHIM}$
1	58	83	3*
2	24	36	0

* not found at wean

c

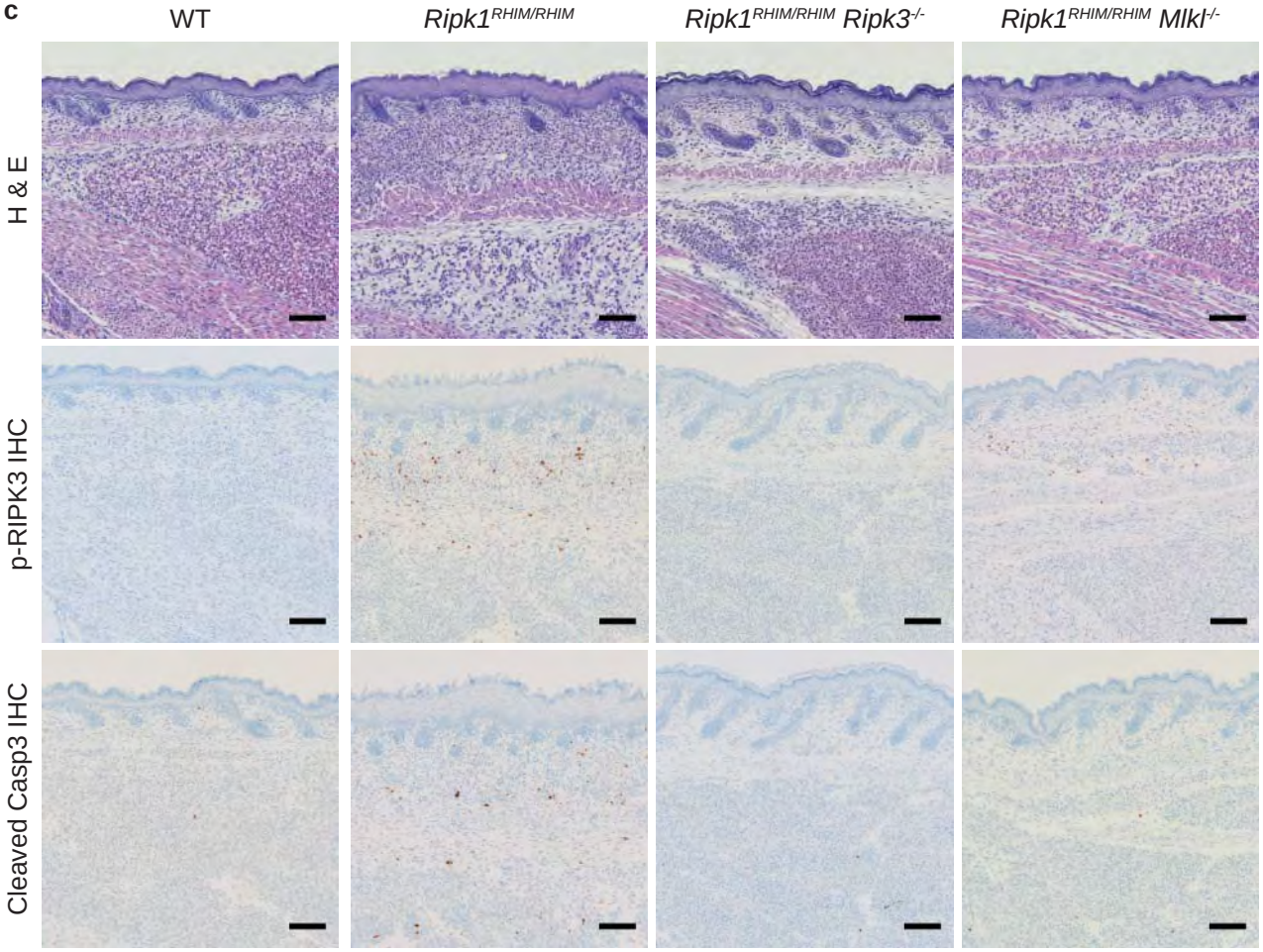

d

	Ripk1$^{+/+}$	*Ripk1*$^{+/RHIM}$	*Ripk1*$^{RHIM/RHIM}$
Ripk3$^{+/+}$	15	18	0
Ripk3$^{+/-}$	32	44	27
Ripk3$^{-/-}$	16	24	10

e

	Ripk1$^{+/+}$	*Ripk1*$^{+/RHIM}$	*Ripk1*$^{RHIM/RHIM}$
Mlkl$^{+/+}$	4	21	0
Mlkl$^{+/-}$	20	36	0
Mlkl$^{-/-}$	8	21	12

f

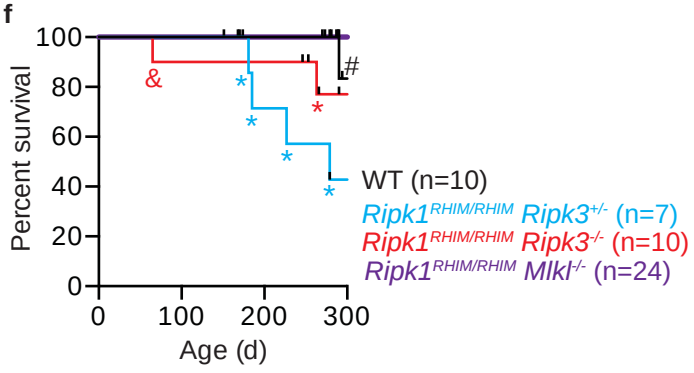

Figure 1

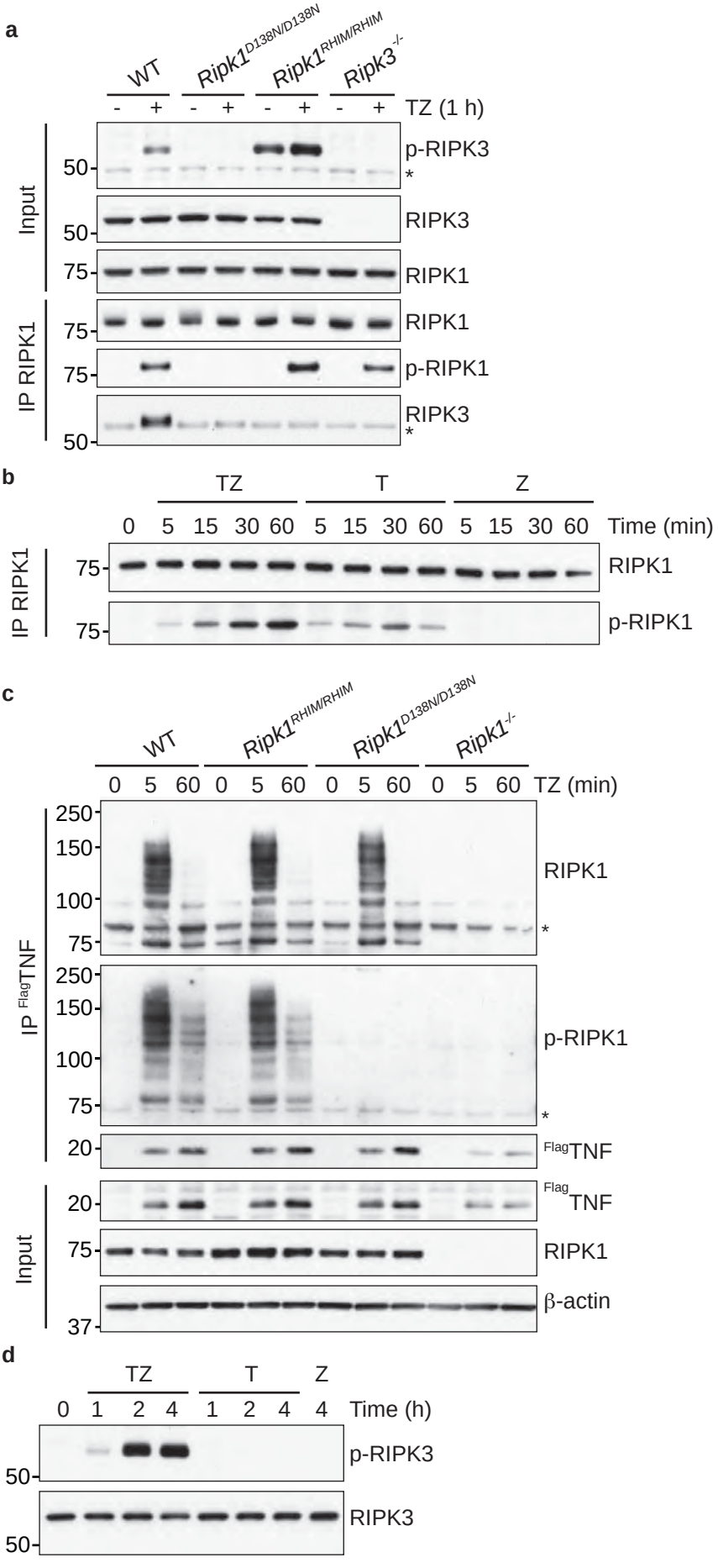
a
WT
Ripk1D138N/D138N
Ripk1RHIM/RHIM
Ripk3-/-
- + - + - + - +
TZ (1 h)
Input
IP RIPK1
p-RIPK3
RIPK3
RIPK1
p-RIPK1
50
75
b
TZ
T
Z
0 5 15 30 60 5 15 30 60 5 15 30 60
Time (min)
c
WT
Ripk1RHIM/RHIM
Ripk1D138N/D138N
Ripk1-/-
0 5 60 0 5 60 0 5 60 0 5 60
TZ (min)
IP FlagTNF
FlagTNF
β-actin
250
150
100
20
37
d
TZ
T
Z
0 1 2 4 1 2 4 4
Time (h)

Figure 2

a

	Ripk1$^{+/+}$	*Ripk1*$^{+/-}$	*Ripk1*$^{-/-}$
Casp8$^{+/+}$	21	69	3
Casp8$^{+/-}$	68	125	17
Casp8$^{-/-}$	0	0	26

b

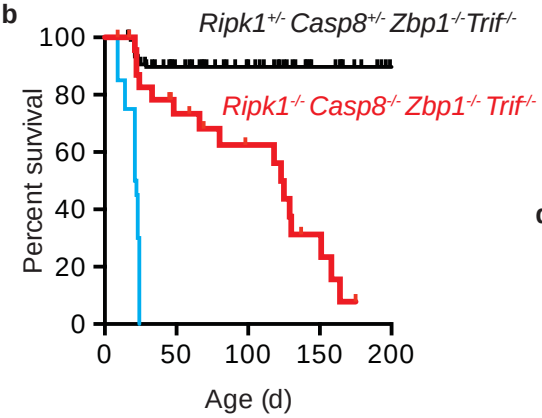

Ripk1$^{-/-}$ *Casp8*$^{+/-}$ *Zbp1*$^{-/-}$ *Trif*$^{-/-}$
or *Ripk1*$^{-/-}$ *Casp8*$^{+/+}$ *Zbp1*$^{-/-}$ *Trif*$^{-/-}$

c

Ripk1$^{-/-}$ *Casp8*$^{-/-}$ *Zbp1*$^{-/-}$ *Trif*$^{-/-}$

Ripk1$^{+/-}$ *Casp8*$^{+/-}$ *Zbp1*$^{-/-}$ *Trif*$^{-/-}$

d

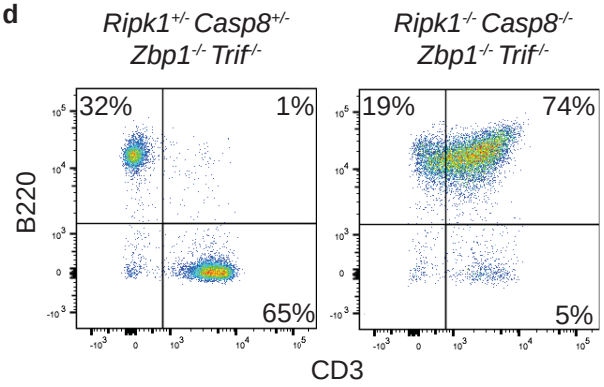

e

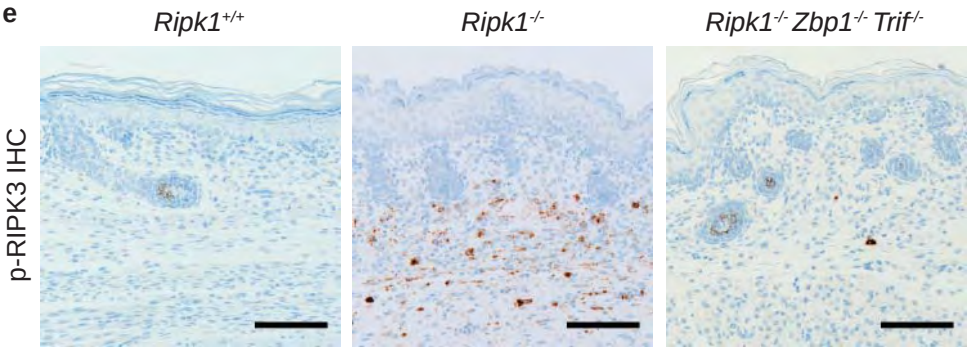

Figure 3

a

	Ripk1$^{+/+}$	*Ripk1*$^{+/RHIM}$	*Ripk1*$^{RHIM/RHIM}$
Zbp1$^{+/+}$	7	12	0
Zbp1$^{+/-}$	8	22	0
Zbp1$^{-/-}$	4	9	7

b

	Ripk1$^{+/+}$	*Ripk1*$^{+/RHIM}$	*Ripk1*$^{RHIM/RHIM}$
Trif$^{+/+}$	8	12	0
Trif$^{+/-}$	22	35	0
Trif$^{-/-}$	7	7	0

c

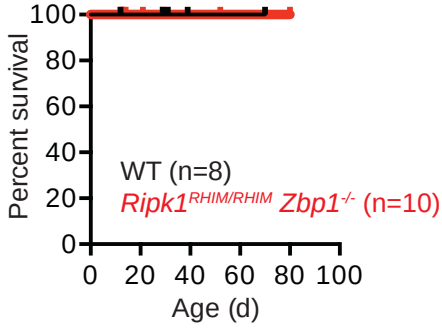

d

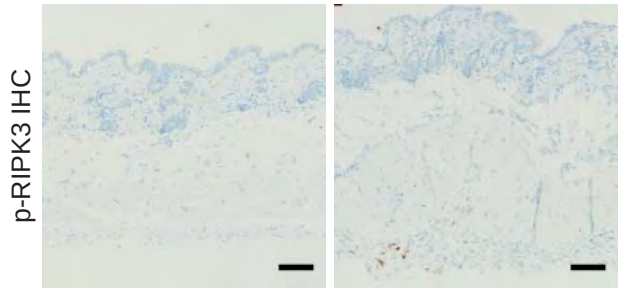

e

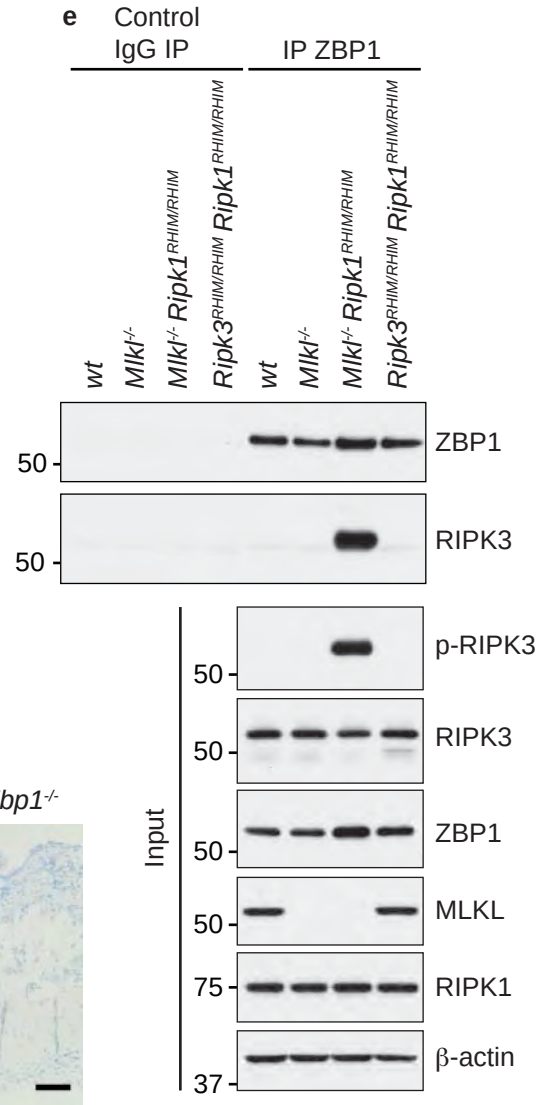

be good to include RHIM KI TRIF KO ZBP1 KO too
from TH16-1135(4)

Figure 4

Extended data figure 1

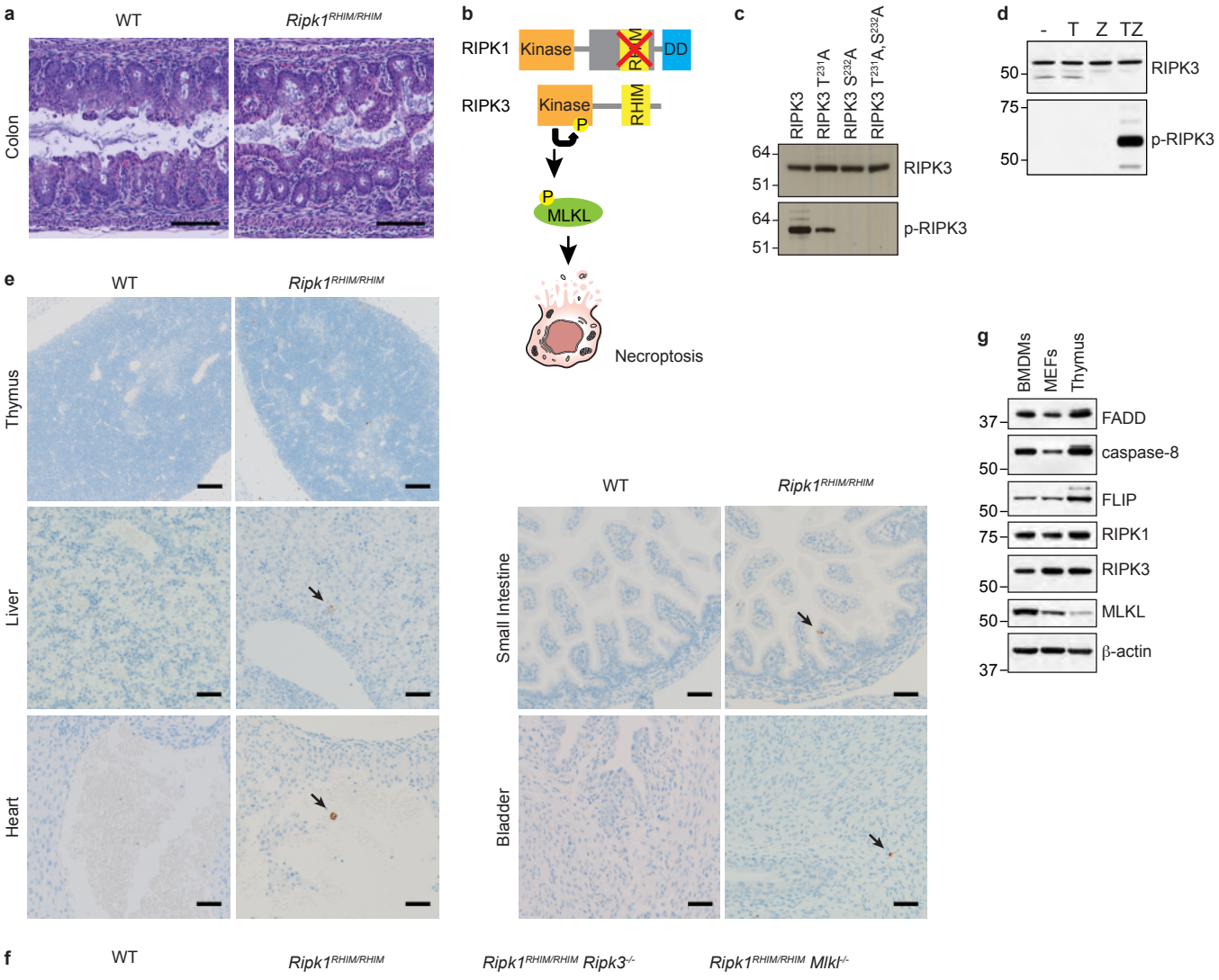

TUNEL stain on E18.5 skin and thymus pending....

Extended data figure 2

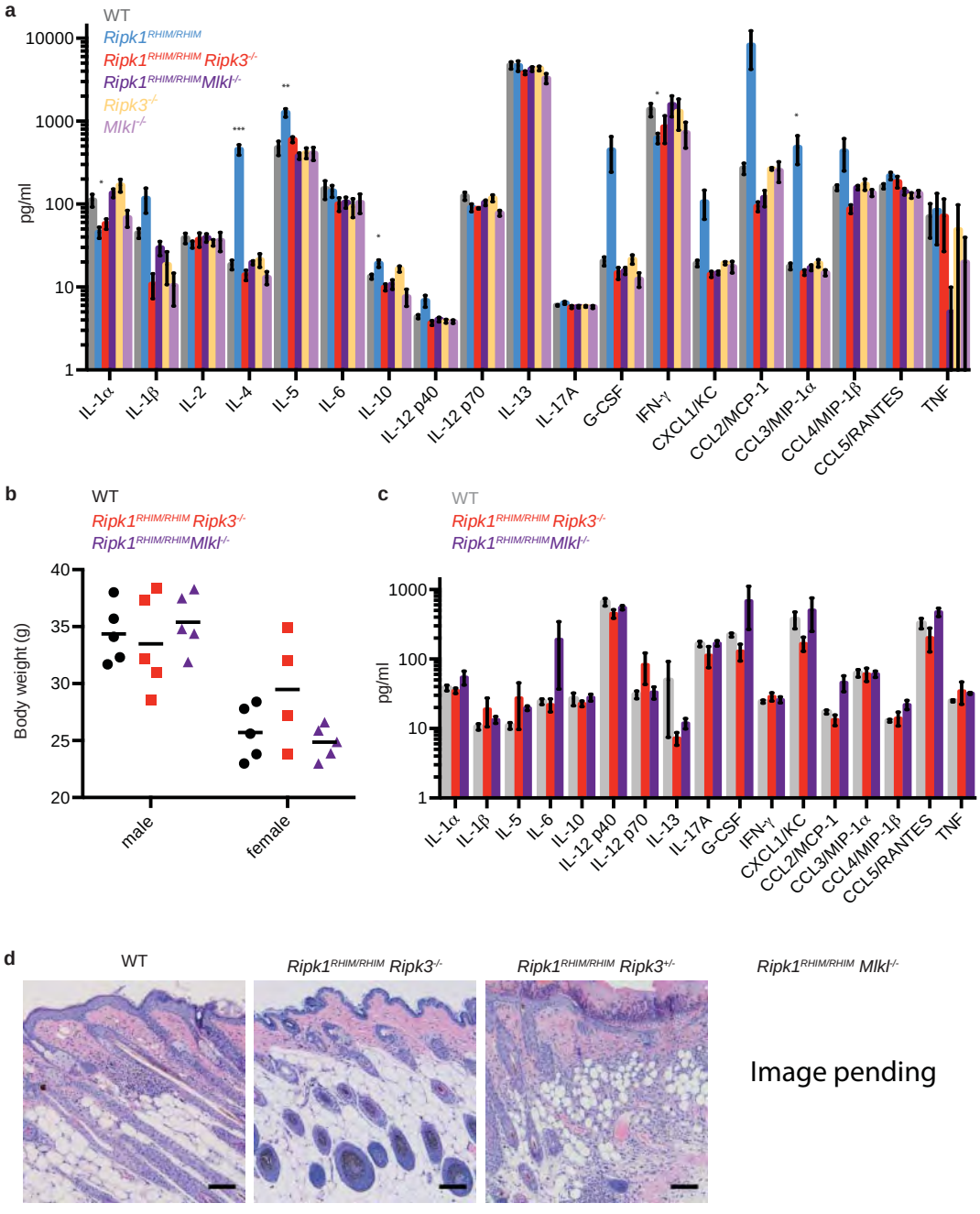

numbers updated 8/17/16

Extended data figure 3

a

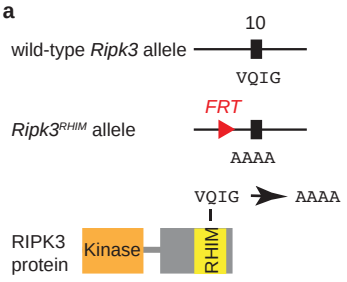

b

	Ripk1$^{+/+}$	*Ripk1*$^{+/RHIM}$	*Ripk1*$^{RHIM/RHIM}$
Ripk3$^{+/+}$	11	21	0
Ripk3$^{+/RHIM}$	17	41	23
Ripk3$^{RHIM/RHIM}$	11	14	3

c

	Ripk1$^{+/+}$	*Ripk1*$^{+/RHIM}$	*Ripk1*$^{RHIM/RHIM}$
Ripk3$^{+/+}$	20	26	0
Ripk3$^{+/D161N}$	33	67	0
Ripk3$^{D161N/D161N}$	0	0	12

d

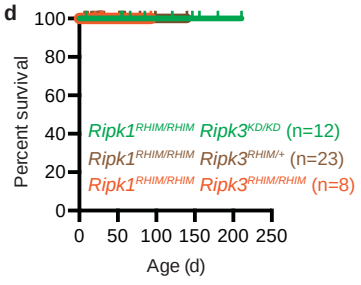

e

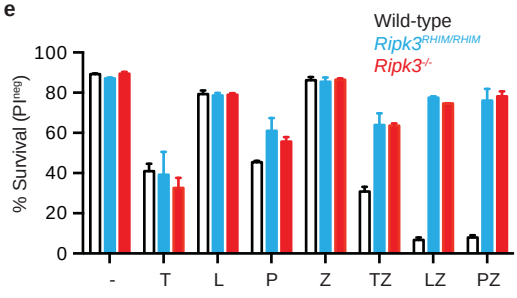

f

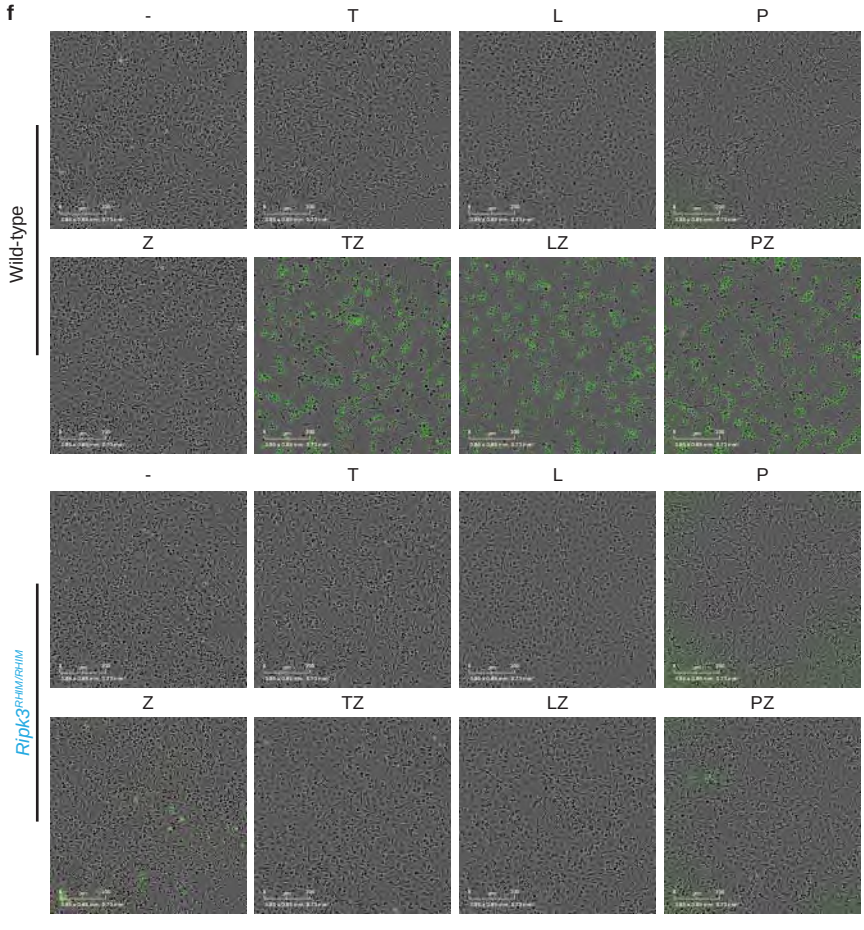

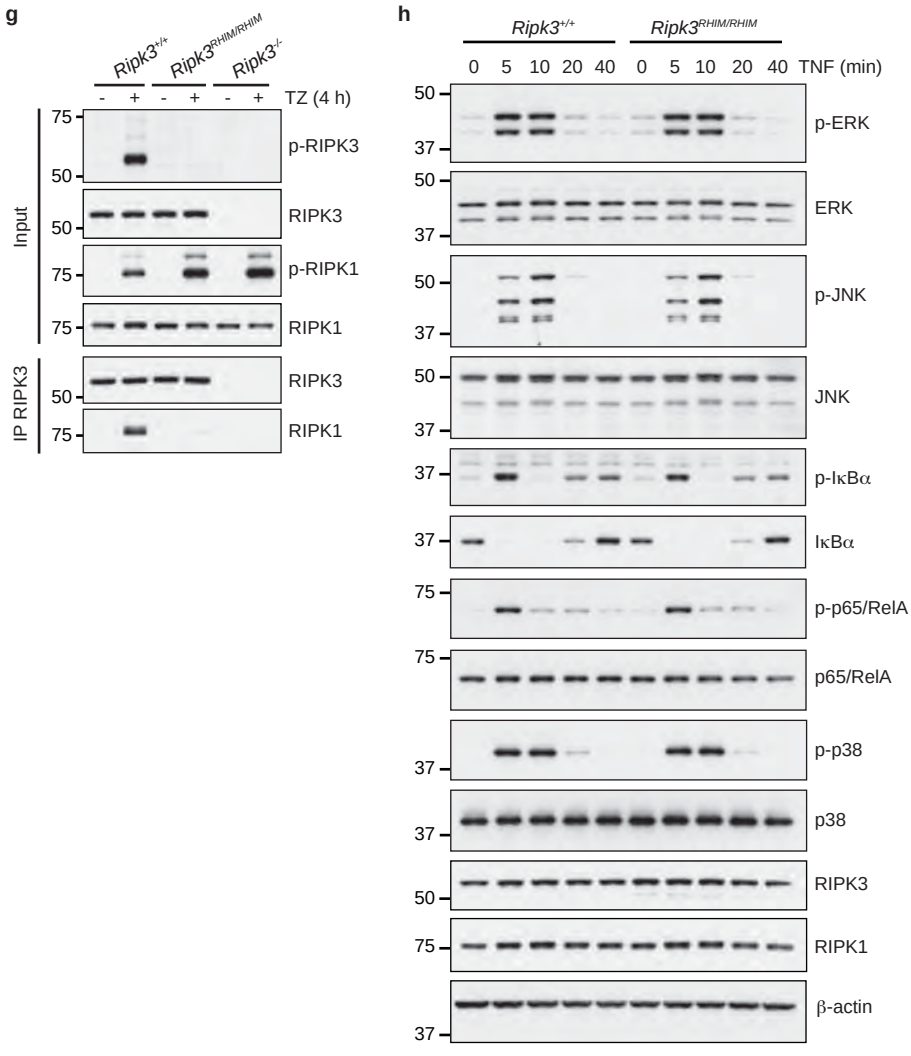
g
Ripk3+/+
Ripk3RHIM/RHIM
Ripk3-/-
- + - + - +
TZ (4 h)
Input
IP RIPK3
75
50
50
75
50
75
p-RIPK3
RIPK3
p-RIPK1
RIPK1
RIPK3
RIPK1
h
Ripk3+/+
Ripk3RHIM/RHIM
0 5 10 20 40 0 5 10 20 40 TNF (min)
50
37
50
37
50
37
50
37
37
37
75
75
37
37
50
75
37
p-ERK
ERK
p-JNK
JNK
p-IκBα
IκBα
p-p65/RelA
p65/RelA
p-p38
p38
RIPK3
RIPK1
β-actin

Extended data figure 4

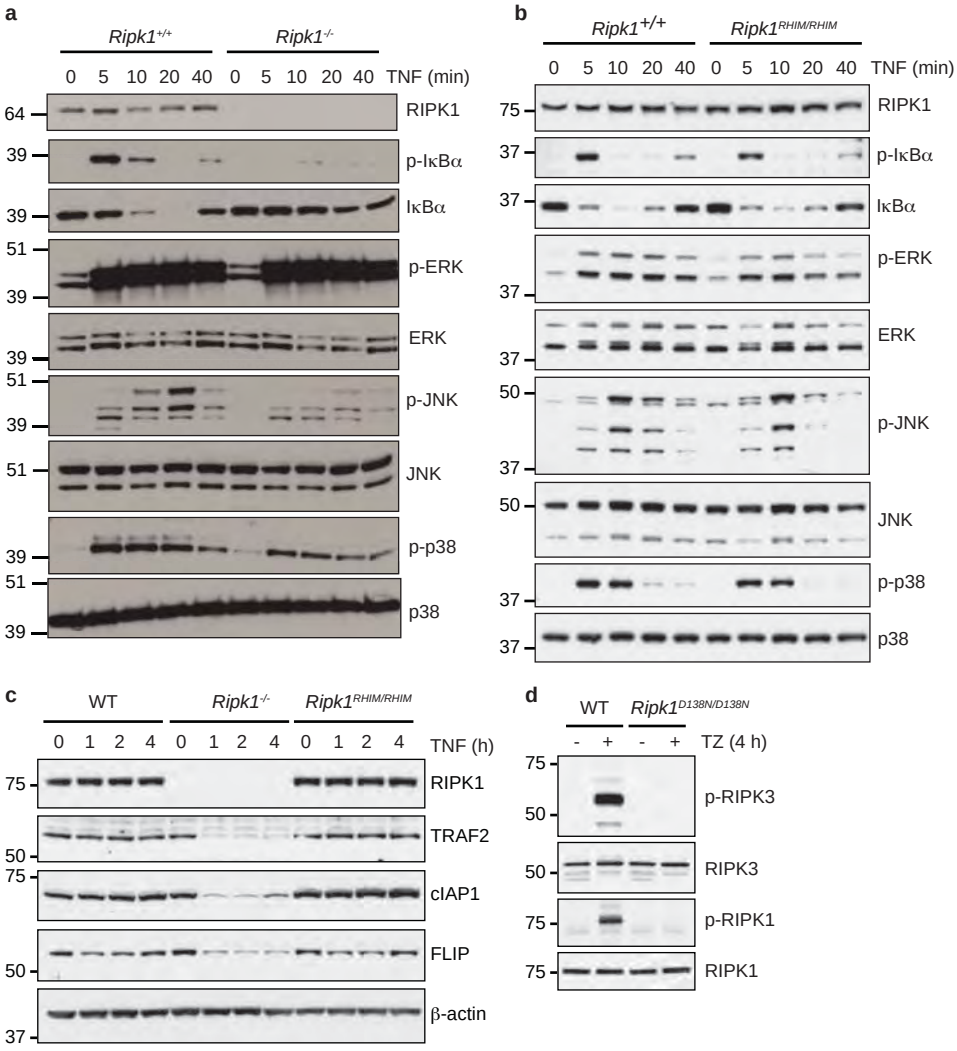

Extended data figure 5

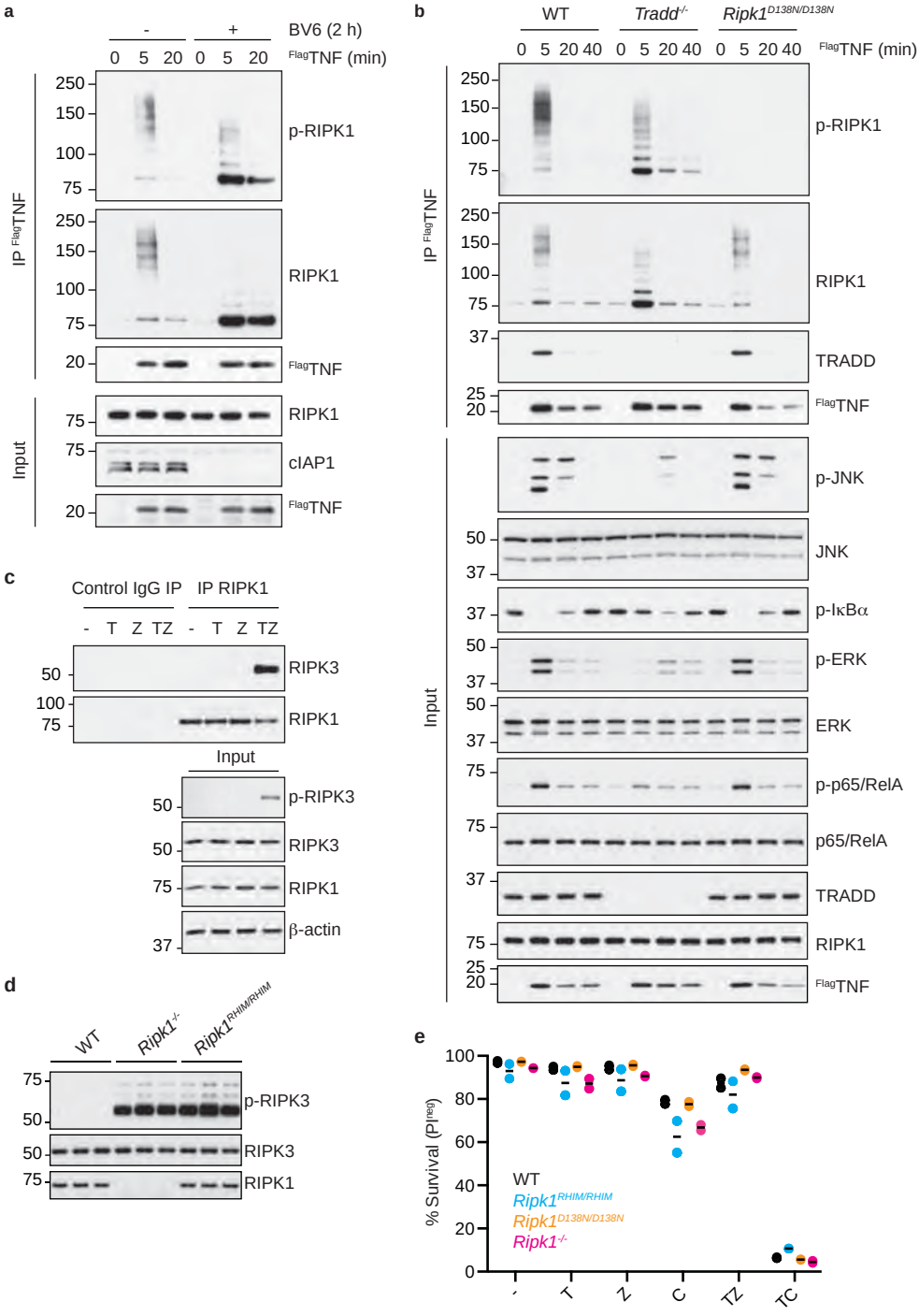

Extended data figure 6

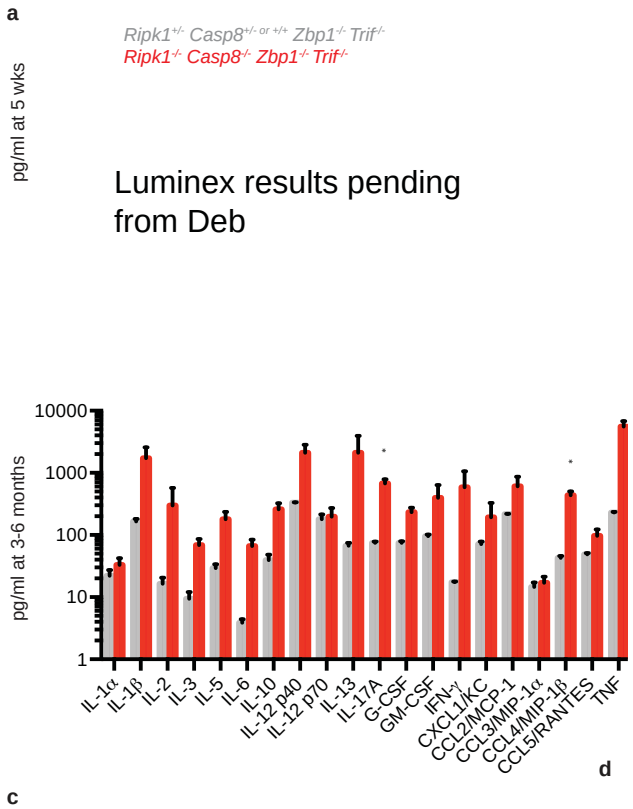

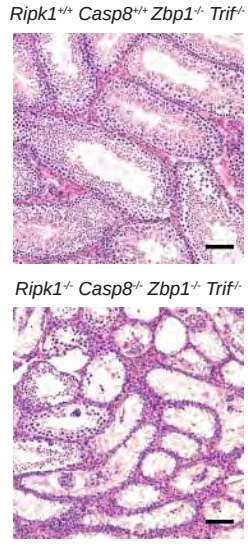

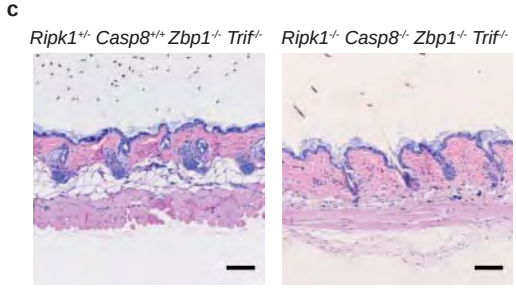

TKO histology pending from TH16-1135(6)

Extended data figure 7

a *Trif*$^{-/-}$ *Ripk1*$^{RHIM/RHIM}$ *Trif*$^{-/-}$

E18.5 skin histology pending...
From TH16-2081(1).

b WT *Ripk1*$^{RHIM/RHIM}$ *Zbp1*$^{-/-}$

Skin WBs pending

c

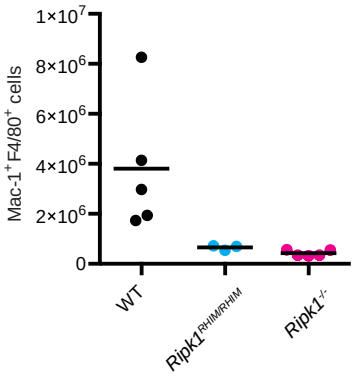

d

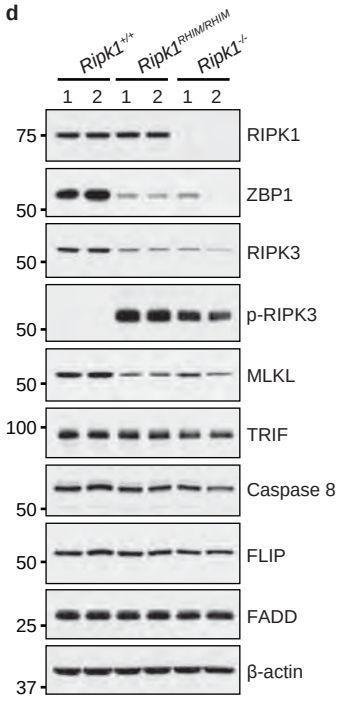

e

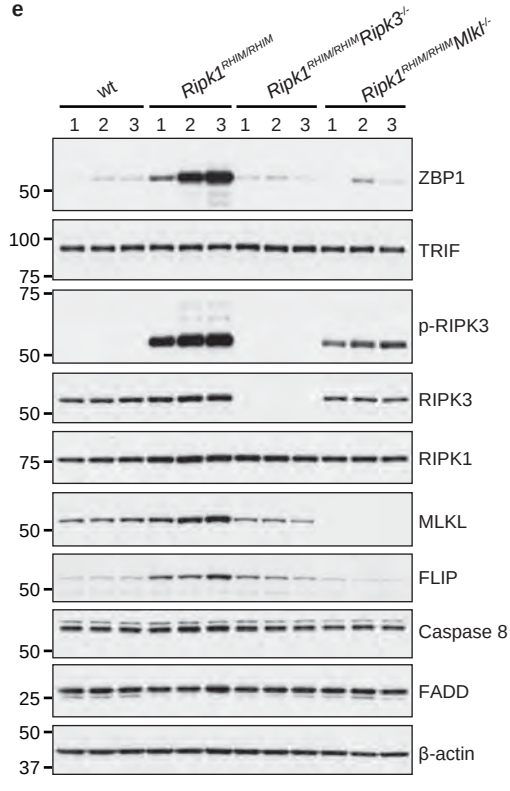

f

taqman
data for ifna/b
pending